Report

Cell Reports

Apolipoprotein E Regulates Amyloid Formation within Endosomes of Pigment Cells

Graphical Abstract

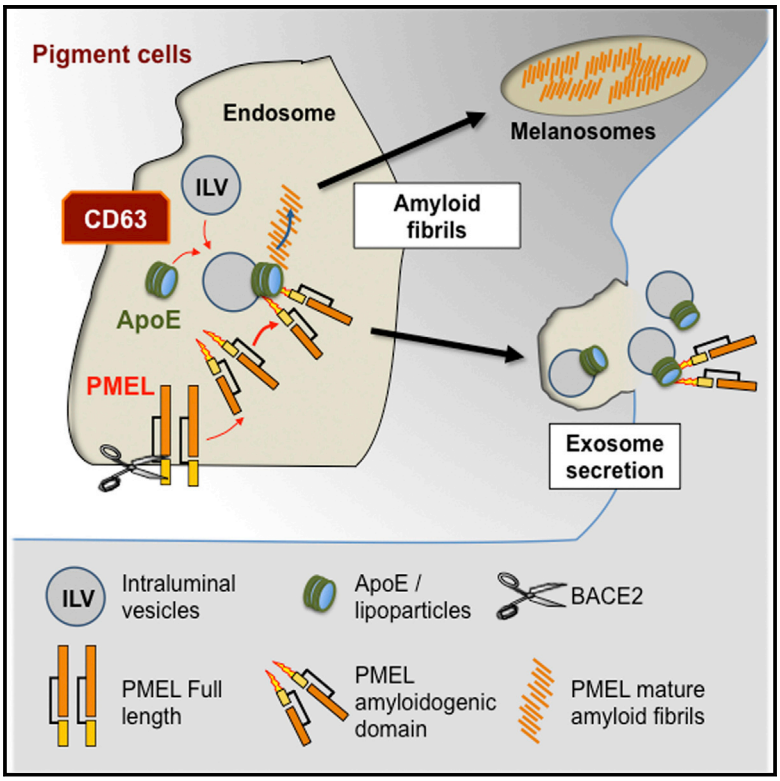

Highlights

- Exosomes and endosomal intraluminal vesicles are associated with ApoE
- ApoE regulates the formation of PMEL amyloid fibrils in endosomes
- ApoE supports the ESCRT independent sorting of PMEL to ILVs

Authors

Guillaume van Niel, Ptissam Bergam, Aurelie Di Cicco, ..., Damarys Loew, Daniel Levy, Graça Raposo

Correspondence

guillaume.van-niel@curie.fr

In Brief

Amyloids are protein aggregates that can be cytotoxic. van Niel et al. showed that Apolipoprotein E, a key factor involved in the metabolism of these pathological amyloids, regulates the formation in a non-toxic manner of amyloid structures that serves physiological functions in specialized cells.

van Niel et al., 2015, Cell Reports *13*, 43–51
October 6, 2015 ©2015 The Authors
http://dx.doi.org/10.1016/j.celrep.2015.08.057

Cell Reports
Report

Apolipoprotein E Regulates Amyloid Formation within Endosomes of Pigment Cells

Guillaume van Niel,[1,2,3,*] Ptissam Bergam,[1,2,3] Aurelie Di Cicco,[3,4,5] Ilse Hurbain,[1,2,3] Alessandra Lo Cicero,[1,2] Florent Dingli,[6] Roberta Palmulli,[1,2] Cecile Fort,[1,2] Marie Claude Potier,[7] Leon J. Schurgers,[8] Damarys Loew,[6] Daniel Levy,[3,4,5,9] and Graça Raposo[1,2,3,9]

[1]Institut Curie, PSL Research University, UMR144, Centre de Recherche, 26 rue d'ULM, Paris 75231, France
[2]Centre National de la Recherche Scientifique, UMR144, Paris 75248, France
[3]Cell and Tissue Imaging Core Facility PICT-IBiSA, Institut Curie, Paris 75248, France
[4]Institut Curie, PSL Research University, UMR168, Centre de Recherche, 26 rue d'ULM, Paris 75231, France
[5]Centre National de la Recherche Scientifique, UMR 168, Paris 75231, France
[6]Institut Curie, PSL Research University, Centre de Recherche, Laboratoire de Spectrométrie de Masse Protéomique, Paris 75248, France
[7]Institut du Cerveau et de la Moelle, CNRS UMR7225, INSERM U1127, UPMC Hôpital de la Pitié-Salpêtrière, 47 Bd de l'Hôpital, Paris 75013, France
[8]Department of Biochemistry, Cardiovascular Research Institute Maastricht, P.O. Box 616, 6200 MD Maastricht, the Netherlands
[9]Co-senior author
*Correspondence: guillaume.van-niel@curie.fr
http://dx.doi.org/10.1016/j.celrep.2015.08.057

SUMMARY

Accumulation of toxic amyloid oligomers is a key feature in the pathogenesis of amyloid-related diseases. Formation of mature amyloid fibrils is one defense mechanism to neutralize toxic prefibrillar oligomers. This mechanism is notably influenced by *apolipoprotein E* variants. Cells that produce mature amyloid fibrils to serve physiological functions must exploit specific mechanisms to avoid potential accumulation of toxic species. Pigment cells have tuned their endosomes to maximize the formation of functional amyloid from the protein PMEL. Here, we show that ApoE is associated with intraluminal vesicles (ILV) within endosomes and remain associated with ILVs when they are secreted as exosomes. ApoE functions in the ESCRT-independent sorting mechanism of PMEL onto ILVs and regulates the endosomal formation of PMEL amyloid fibrils in vitro and in vivo. This process secures the physiological formation of amyloid fibrils by exploiting ILVs as amyloid nucleating platforms.

INTRODUCTION

Amyloids oligomers and fibrils are broadly associated with various diseases including Alzheimer disease (AD) among others (Harrison et al., 2007). Yet, the process of amyloid formation and the role they play in the physiopathology of disease remains unclear. Of interest, there is accumulating evidence for the involvement of endosomal compartments in amyloid homeostasis (Thinakaran and Koo, 2008). In particular, amyloidogenic proteins and peptides accumulate in multivesicular endosomes (MVEs) and aggregate as toxic oligomers (Takahashi et al., 2002). These endosomal aggregates cause neuronal lysis (D'Andrea et al., 2001) that contributes to the release of toxic species into the extracellular space (Haass and Selkoe, 2007). A cell defense mechanism to neutralize these toxic species is their incorporation into more inert mature amyloid fibrils (Haass and Selkoe, 2007). The fibrillation process is notably influenced by lipoparticles containing the apolipoprotein E (ApoE) (Kanekiyo et al., 2014), variants of which are major genetic risk factors for AD.

Yet, not all amyloids are associated with disease as so-called "functional" amyloids (Fowler et al., 2007) serve physiological roles. The best studied example of functional amyloids in mammals is amyloid fibrils produced from amyloidogenic fragments of the premelanosomal protein (PMEL) in pigment cells (Watt et al., 2013). These amyloid fibrils serve as a scaffold on which melanins polymerize within lysosome-related organelles called melanosomes (Raposo and Marks, 2007). The unique mechanisms exploited by pigment cells to avoid accumulation of potentially toxic amyloidogenic fragments of PMEL in MVEs remain elusive (Watt et al., 2011, 2013). Yet, the sorting of PMEL amyloidogenic fragments to intraluminal membrane vesicles (ILVs) seem crucial to induce their aggregation into inert "functional" amyloid fibrils (van Niel et al., 2011). During this process, the PMEL lumenal amyloidogenic fragment is released by a beta-secretase BACE-2-mediated cleavage (Rochin et al., 2013) from a C-terminal fragment (CTF) (Kummer et al., 2009; van Niel et al., 2011) and, within the same MVE, is sorted to the intraluminal vesicles (ILVs) by an endosomal sorting complex required for transport (ESCRT)-independent/CD63-dependent mechanism (van Niel et al., 2011). Here, we show that ILVs of MVEs function as nucleating platforms for amyloid fibrillogenesis, and ApoE at the membrane of ILVs plays a pivotal role in PMEL sorting and in the formation of PMEL fibrils.

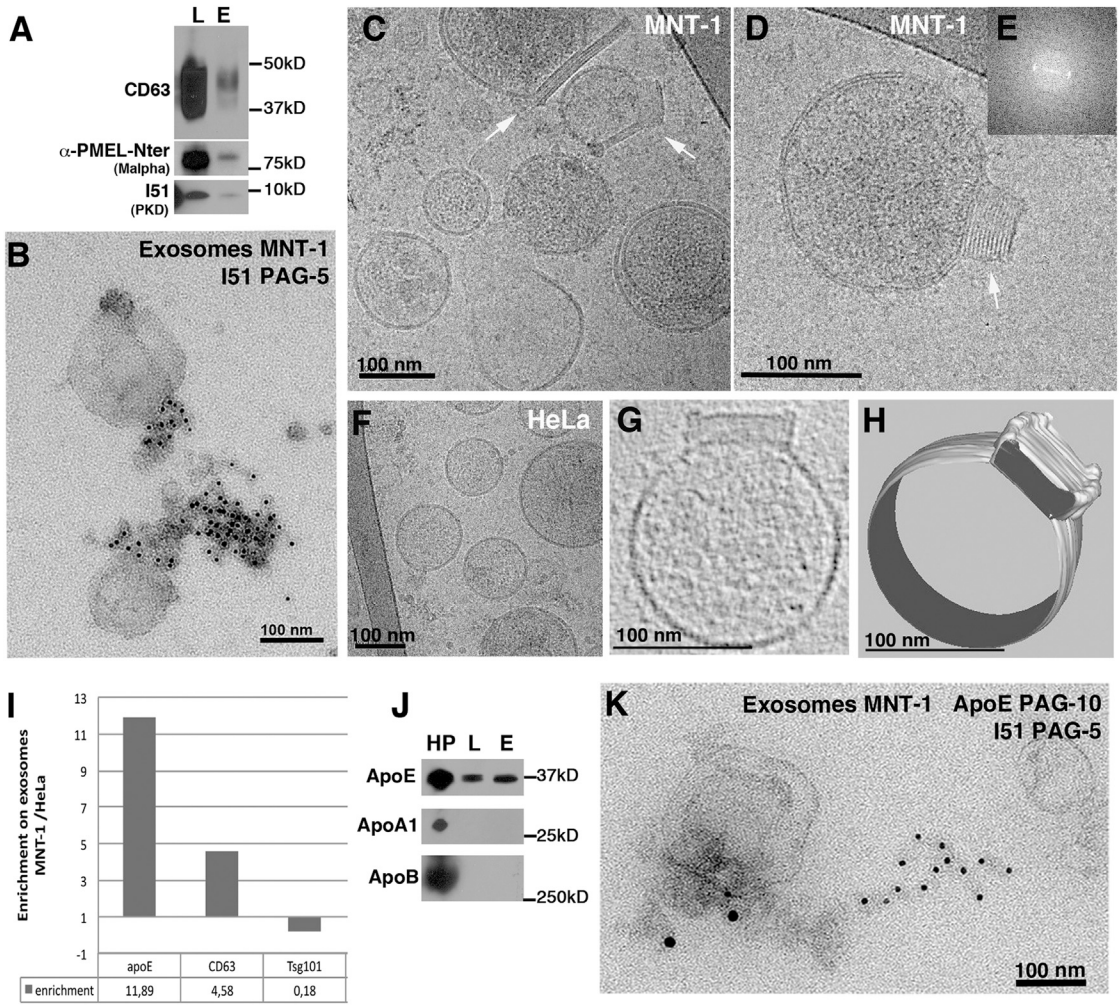

Figure 1. Identification and Characterization of Exosomes from MNT-1 Cells

(A) Lysates (L) and exosomes (E) isolated from medium of MNT-1 cells were analyzed by western blot for CD63, PMEL luminal domain full length (α-PMEL-Nter), and PMEL amyloidogenic fragment (I51).

(B) Exosomes from MNT-1 were immunolabeled with antibodies against PMEL amyloidogenic fragment (I51), revealed with Protein A gold particles (PAG) of 5 nm diameter and observed by EM.

(C–H) Analysis of exosomes by cryo-EM. (C and D) Exosomes purified from MNT-1 cells culture media. Some exosomes are covered by a cap made of a stack of layers (white arrows). (E) Fourier transform of the stack of layers observed in (D) showing diffraction spots at 1/3.5 nm. (F) Exosomes purified from HeLa cells. (G and H) 3D reconstruction of MNT-1 exosomes by cryotomography and corresponding 3D model.

(I) The presence of ApoE, CD63, and Tsg101 in equivalent amount of exosomes from MNT-1 and HeLa cells was determined from western blot analysis (shown in Figure S1H) and their enrichment in MNT-1-derived exosomes was quantified and normalized to their enrichment in exosomes from HeLa cells without cap.

(J) Human Plasma (HP), lysates (L) and exosomes (E) from MNT-1 cells were analyzed by western blot for ApoE, ApoA1, and ApoB.

(K) Exosomes from MNT-1 were co-immunolabeled with antibodies against PMEL amyloidogenic fragment (I51, PAG 15) and ApoE (PAG 10).

See also Figure S1.

RESULTS

Exosomes from Pigment Cells Are Associated with ApoE Lipoparticles

To better understand the involvement of ILVs in the formation of amyloids, we first investigated the fraction of ILVs secreted as exosomes from pigment cells. Exosomes are extracellular ILVs that are released after the fusion of MVEs with the plasma membrane (Raposo and Stoorvogel, 2013). They are enriched in specific sets of lipids, proteins, and RNAs and provide details on key processes in MVEs from which they originate. Exosomes isolated from culture medium of human melanocytic cell line MNT-1 contained the tetraspanin CD63 that is commonly enriched in MVEs and exosomes. The exosome pellet also contained processed and full-length amyloidogenic luminal domain of PMEL (Figure 1A) and the PMEL CTF and the melanosomal protein MART-1 (Figure S1A). The distinct intra-endosomal trafficking of PMEL CTF and luminal domain (van Niel et al., 2011) and the absence of interaction between both fragments (Figure S1B) indicated that the PMEL luminal domain is likely

associated with exosomes after release from the CTF. By immunoelectron microscopy (IEM), the processed PMEL amyloidogenic domain associated as aggregates with the outer membrane of 100–150 nm vesicles (Figure 1B). These observations suggested that these exosomes are the extracellular counterpart to the ILVs upon which PMEL amyloid fibrils formed within MVEs. We next analyzed MNT-1 exosomes at high resolution by cryoelectron microscopy (cryo-EM). Exosomes appeared as a population of spherical vesicles of 120 nm diameter on average with few larger vesicles as previously reported (Brouwers et al., 2013; Ji et al., 2013). The vesicles displayed two layers of electronic densities 3.5–4 nm apart, corresponding to each leaflet of the lipid bilayer and were covered by darker densities that correspond to membrane proteins (Figure 1C). Surprisingly, ~10% of MNT-1 exosomes exhibited a "cap" consisting of a stack of horizontal layers (Figures 1C and 1D). Most caps were rectangular by thin section but some were conical (Figures S1D and S1E) and their dimensions range between 12–38 nm in height and 30–100 nm in width (Figures 1C and S1C–S1E). The number of layers varied from 4 to 12, but the distance between each layer was constant to 3.5 nm, as shown by the diffraction spots present in the Fourier transform (Figure 1E, inset). Analysis of the exosomes by cryotomography revealed that the caps had a closed cylindrical shape in three dimensions (Figures 1G and 1H). Such caps were also observed on exosomes from primary melanocyte cells but not on exosomes from HeLa (Figure 1F) and other cell types (Figure S1F).

The stacked layers and spacing of the MNT-1 exosome caps were strikingly reminiscent of low-density lipoproteins consisting of apolipoproteins and cholesterol forming a striated core with layers spaced by 30–35 Å and observed by cryo-EM (Orlova et al., 1999). Using quantitative mass spectrometry (SILAC) we compared exosomes derived from either unlabeled MNT-1 cells or HeLa cells cultured in heavy media. In the genome ontology (GO) term 0034358 "Plasma lipoprotein particle," only human ApoE was found statistically enriched in exosomes derived from MNT-1 (enrichment factor: 4.30, p value = 1.08e-03, 25 specific peptides with a coverage >61%) in agreement with endogenous expression of *APOE* in pigment cell type (Ishida et al., 2004).

Western blot analysis of exosomes released from MNT-1 cells further shows that ApoE was enriched (Figures 1I and S1G) and that apolipoproteins A1 and B were absent (Figure 1J), excluding potential contamination by plasma lipoparticles. Moreover, floatation of exosomes on sucrose gradient showed that ApoE was only present in the fraction containing exosome-associated proteins, thereby excluding free ApoE or ApoE-lipoparticles in the exosomal pellet (Figure S1H). Using cryo-EM and immunogold labeling we strengthen the findings that ApoE is associated with exosomes (Figure 1L). Immunogold labeling on aldehyde-fixed exosomes highlights the co-localization of ApoE on the outer membrane of exosomes with CD63 (Figure S1I) and PMEL fibrils (Figure 1K). Similar observations were done on exosomes derived from human primary melanocytes (Figures S1J and S1K).

Endogenous ApoE Co-localizes and Interacts with PMEL on ILVs of Endosomes

The endosomal origin of exosomes led us to investigate whether ApoE is present within MVEs. Endogenous ApoE was detected by western blotting of lysates of MNT-1 cells grown in lipoprotein-depleted human serum (LPDS) and was significantly reduced after treatment with ApoE-specific small interfering RNA (siRNA) (Figure 2A). By immunofluorescence microscopy, labeling for PMEL and ApoE partially overlapped in post-Golgi compartments of MNT-1 cells grown in LPDS (Figure 2B), and IEM analyses detected ApoE in MVEs and in early stage melanosomes containing PMEL-derived fibrils (Figure 2C). The association of ApoE with ILVs was confirmed by cell fractionation on sucrose gradients, in which CD63, PMEL amyloidogenic fragments, and ApoE were enriched in a fraction of similar density to that of exosomes (Figure S2A, fraction 3). IEM analysis of this fraction revealed membrane vesicles enriched in CD63 (Figures 2D and 2E) that were of similar diameter and orientation as the exosomes described above. These ILVs associated with PMEL fibrils (Figures 2D and S2B) and ApoE-positive structures (Figures 2E and 2F). The co-localization of ApoE and PMEL on ILVs was consistent with their co-immunoprecipitation using antibodies against the luminal domain and amyloidogenic region of PMEL (Figure 2G). These data indicate that ApoE is associated with the PMEL amyloid luminal domain and PMEL fibrils at the surface of ILVs within MVEs.

ApoE Regulates PMEL Amyloid Fibrils Formation

The reported role of ApoE in pathological amyloidogenesis (Kanekiyo et al., 2014) prompted us to investigate the capacity of ApoE to regulate PMEL fibrillogenesis within MVEs of MNT-1 cells. Depletion of endogenous ApoE by siRNA, but not of exogenous ApoE using LPDS (Figure 3A), strongly reduced both the formation of epitopes associated with amyloid fibrils (Figure 3A) and the accumulation of PMEL fibrils in unpigmented stage II melanosomes observed by EM (Figures 3B and 3C). Instead of forming structured fibrils, the PMEL luminal domain in ApoE siRNA-treated cells accumulated as unstructured aggregates within vacuolar structures (Figures S3A and S3B). Consequently, relative to control cells the number of stage III and IV melanosomes with melanin pigments deposited along the fibrils (Seiji et al., 1963) was reduced and aberrant multilamellar structures with irregular lumenal pigment deposits appeared (Figures 3B and 3C, noted "APM," and S3A). Despite the altered morphology of melanosomes, ApoE siRNA did not affect total melanin content (Figure S3C), suggesting that the effect was uniquely associated to amyloid fibril formation and not melanin synthesis. Similar impairment of generation of PMEL fibrils within early melanosomes was also observed after depletion of endogenous ApoE in human primary melanocytes (Figures 3D and 3E).

To test whether ApoE depletion affects PMEL amyloidogenesis in a physiological context, we analyzed melanosome morphology in pigment cells in *APOE*$^{-/-}$ mice. Compared to control C57BL/6J mice (wild-type [WT]), *APOE*$^{-/-}$ mice did not display any obvious coat color defect (Figure S4A) as reported in *PMEL*$^{-/-}$ mice (Hellström et al., 2011). Because of potential compensatory effects observed in skin melanocytes of mice with melanogenesis defects (Lopes et al., 2007), we focused on retinal pigment epithelium (RPE) in which the compensatory effect is less apparent. Whereas, melanosomes in the RPE of control mice were characteristically ellipsoidal, melanosomes of *APOE*$^{-/-}$ mice were rounder (Figures 4A and 4C), but neither larger nor fewer in

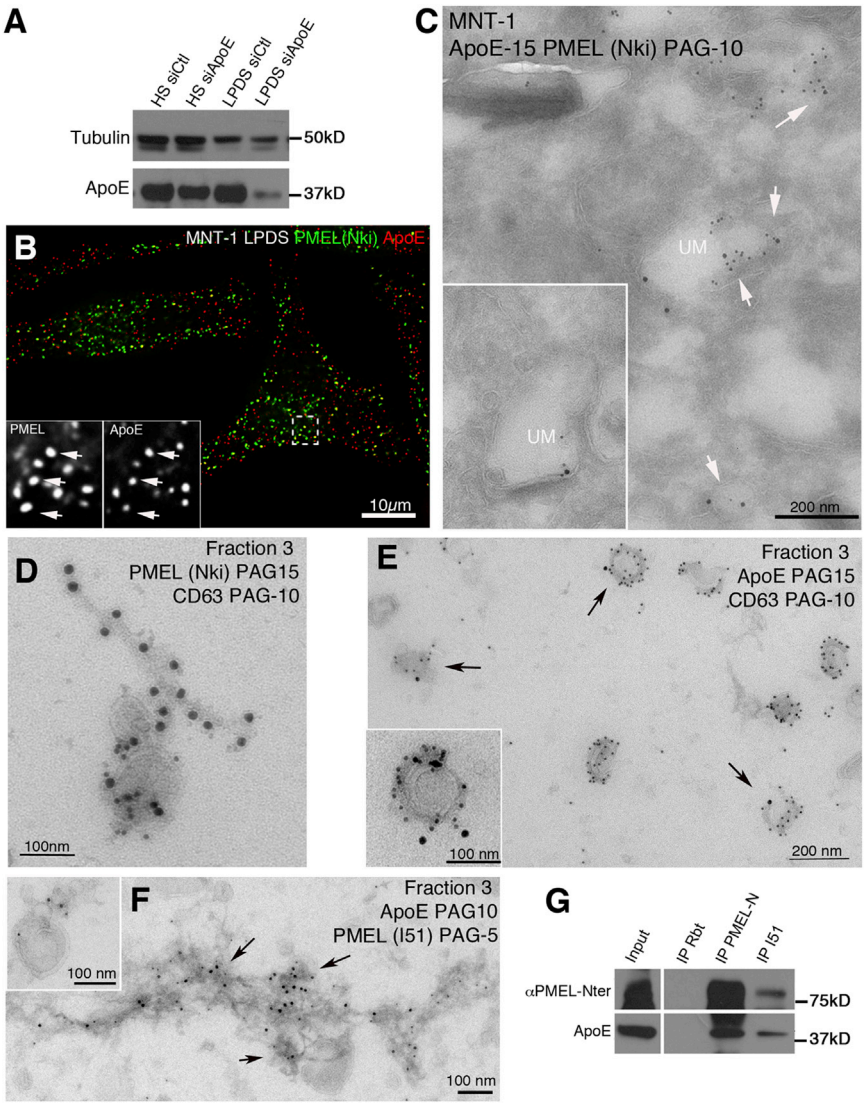

Figure 2. Endosomal Localization of ApoE

(A) Whole cell lysates of MNT-1 cells that were cultured in the presence of human serum (HS) or lipoprotein-depleted human serum (LPDS) and treated with control siRNA or ApoE siRNA were analyzed by western blot using an anti-ApoE antibody or anti-β-tubulin antibody as a loading control.

(B) MNT-1 cells cultured in LPDS were analyzed by IFM after labeling for PMEL luminal domain (Nki) and ApoE; arrows point to co-localization spots.

(C) Ultrathin cryosections of MNT-1 cells were double immunogold labeled for PMEL luminal domain (Nki, PAG 10) and ApoE (PAG 15). Arrows indicate ApoE labeling in unpigmented early melanosomes (UM).

(D–F) Fraction 3 obtained from cell fractionation of MNT-1 cells on sucrose gradients (Figure S2A) was observed by electron microscopy after immunogold labeling with antibodies against (D) PMEL luminal domain (Nki, PAG 15) and CD63 (PAG 10), (E, inset) ApoE (PAG 15) and CD63 (PAG 10), or (E, inset) ApoE (PAG 15) and PMEL amyloidogenic fragment (I51 PAG 5).

(G) TX-100 lysates of MNT-1 cells were immunoprecipitated with isotype control antibody or antibodies specific to PMEL luminal domain full length (α-PMEL-Nter) and PMEL amyloidogenic fragment (I51) as indicated. Immunoprecipitates (IP) or untreated lysate (Input) were analyzed by western blot with α Pmel-N (top) or anti-ApoE antibody (bottom).

See also Figure S2.

number (Figures S4B and S4C). The round shape is characteristic of a defect in PMEL-derived amyloidogenesis as observed in *PMEL*$^{-/-}$ mice (Hellström et al., 2011). Importantly, overexpression of human *APOE3* isoform, and to a lesser extent of human *APOE4* isoform, rescued the phenotype of *APOE*$^{-/-}$ mice (Figures 4B and 4C). In vivo, ApoE- and PMEL-positive labeling were also observed in MVEs of RPE likely corresponding to early stage melanosomes (see electron micrographs in Figures 4D, 4E, and S4D) and on extracellular vesicles that were by their size reminiscent of exosomes in the vicinity of RPE cells (Figures 4F and S4E). These data indicate that ApoE is associated with ILVs and exosomes and is required for PMEL amyloidogenesis and consequently melanosome maturation in vivo.

ApoE Is Involved in the CD63-Dependent/ESCRT-Independent Sorting of PMEL

The defects in melanosome morphology observed in ApoE-deficient melanocytes are reminiscent of those observed when PMEL cleavage or sorting is defective (Rochin et al., 2013; van Niel et al., 2011). Impaired formation of PMEL fibrilogenesis upon ApoE deficiency is not due to a defect of PMEL cleavage since ratio between proteolytic PMEL fragments remained unchanged after ApoE depletion (Figure S5A); but it could be linked to PMEL sorting to ILVs since siRNA-mediated depletion of ApoE reduced the association of ApoE and PMEL luminal domain to ILVs that are released as exosomes (Figure 5A). This defect of PMEL sorting in ApoE-depleted cells echoed the observations made upon depletion of CD63, which regulates the ESCRT-I-independent sorting of the PMEL luminal domain on ILVs (van Niel et al., 2011). In agreement with a role of ApoE and CD63 in the same sorting pathway, partial siRNA-mediated depletion of CD63 (Figure S5B) induced a significant accumulation of ApoE in a perinuclear compartment (Figure 5B) that we identified by EM as the Golgi apparatus (Figure 5C). In contrast, depletion of the ESCRT-I subunit TSG101 (Figure S5B) induced an accumulation of ApoE and PMEL in the lumen of enlarged endosomes with irregular internal membranes (Figures S5C and S5D). As a potential consequence of impaired endosomal trafficking of ApoE, depletion of CD63, but not of ESCRT-I, inhibited the targeting of ApoE to ILVs secreted as exosomes (Figure 5D) and the co-immunoprecipitation of PMEL with ApoE

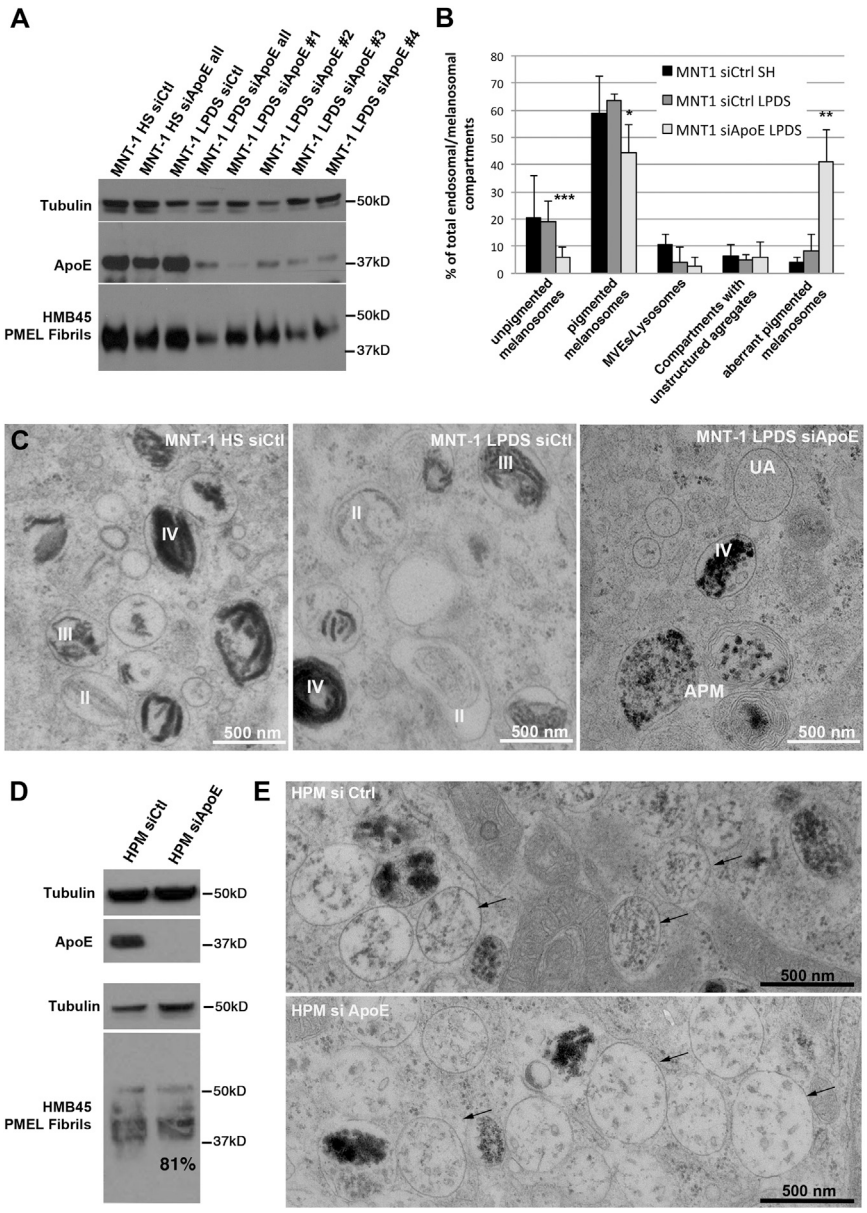

Figure 3. ApoE in the Fibrillogenesis of PMEL in Cell Line

(A) Whole cell lysates of MNT-1 cells that were cultured in HS or LPDS and treated with either control siRNA or different ApoE siRNA were analyzed by western blot with anti-ApoE antibody or anti-β-tubulin antibody as a loading control. Corresponding Triton X-100-insoluble fraction from MNT-1 cells were analyzed by western blot using fibrils-specific antibody HMB45.

(B) Quantification of the number of different endosomal/melanosomal compartments, as indicated on the x axis and defined by morphology, observed by conventional EM in MNT-1 cells that were treated as indicated. Values represent the percentage of each compartment (±SD) relative to all of the endosomal/melanosomal compartments identified in 20 cell profiles per condition (***$p < 0.01$, **$p < 0.02$, *$p < 0.05$).

(C) Control cells cultured in HS and LPDS or in ApoE-depleted cells cultured in LPDS observed by conventional EM. Labels II, III, and IV, indicate the different stages of maturation of melanosomes; UA, unstructured aggregates; APM, aberrant pigmented melanosomes.

(D) Whole cell lysates of human primary melanocytes that were treated with either control siRNA or ApoE siRNA were analyzed by western blot with anti-ApoE antibody or anti-β-tubulin antibody as a loading control. Corresponding Triton X-100 insoluble fractions were analyzed by western blot using fibrils-specific antibody HMB45.

(E) Control and ApoE-depleted human primary melanocytes were observed by conventional EM. Arrows indicate unpigmented early melanosomes that are devoid of PMEL fibrils after ApoE depletion.

See also Figure S3.

(Figure S5E). By contrast, inhibition of sphingomyelinase—that inhibits ESCRT-independent ILV formation in glial cells (Trajkovic et al., 2008) but not PMEL sorting (van Niel et al., 2011)—did not impair ApoE association with exosomes (Figure S5F), indicating that ApoE sorting to ILVs is ceramide-independent. Our results show that ApoE is a downstream effector of the ESCRT-independent/CD63-dependent sorting of PMEL that regulates PMEL amyloidogenesis.

DISCUSSION

Here, we show that the binding of ApoE to the membrane of exosomes and ILVs is a major regulator of PMEL amyloid fibrils formation during melanogenesis. This ascertains *APOE* as a new pigmentation gene, in agreement with the regulation of its expression by MITF, a master regulator of melanocyte development (Hoek et al., 2008). As with other genes required for early steps of melanogenesis (Hellström et al., 2011), *APOE* might have been missed because its disruption causes only minor coat color alterations and no visual defect (Mak et al., 2014) due to potential compensatory mechanisms.

ApoE is an amphipathic protein (Segrest et al., 1992) that could interact both with membranes of ILVs and with the PMEL luminal domain during the processes of sorting and fibrillation. This suggests that ApoE could act as a loading device on ILVs for shed PMEL luminal domain providing a mechanism for the CD63-dependent/ESCRT-independent sorting pathway of PMEL (van Niel et al., 2011). The involvement of CD63 in ESCRT-independent ILVs formation in a cervical cancer cell line (Edgar et al., 2014) and the potential presence of ApoE in exosomes secreted by other cell types such as oligodendrocytes (Conde-Vancells et al., 2008; Krämer-Albers et al., 2007) suggests a widespread mechanism where ApoE could act as a

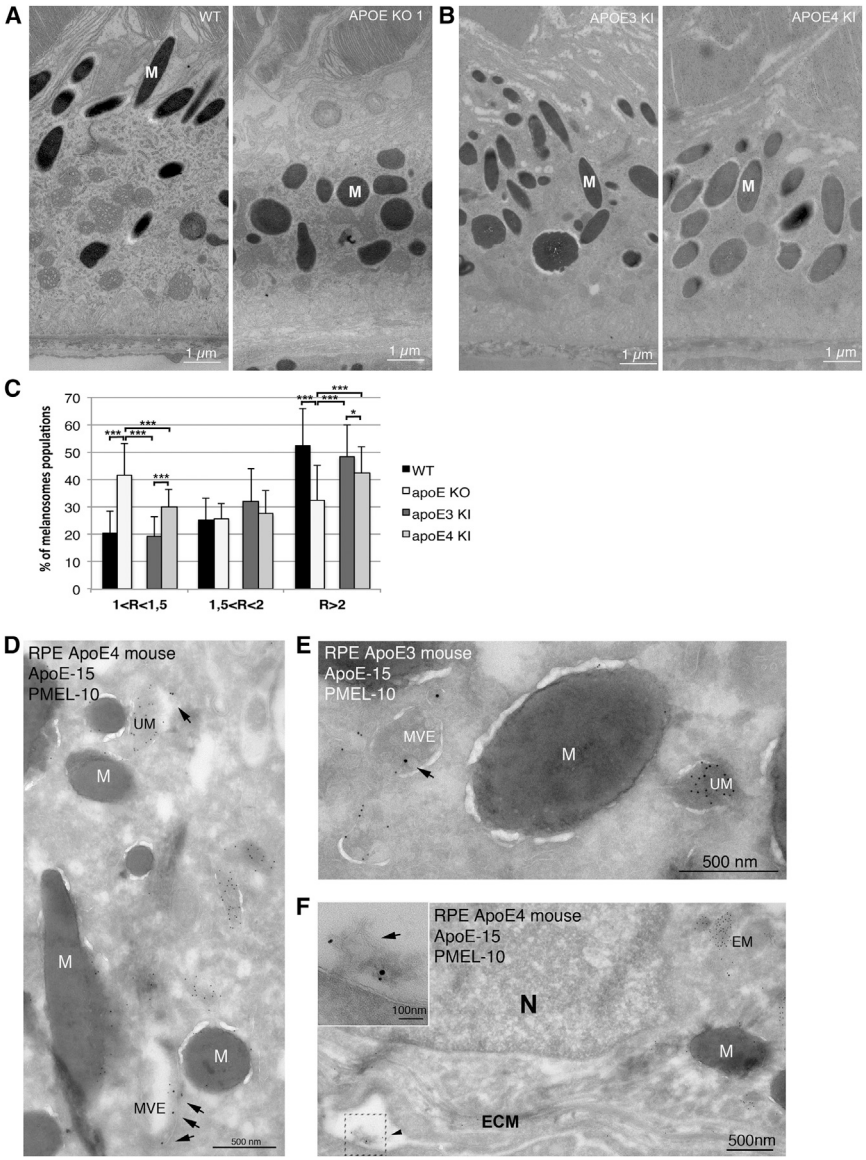

Figure 4. ApoE in the Fibrillogenesis of PMEL In Vivo

(A) RPE sections from *APOE*$^{+/+}$ (left) and *APOE*$^{-/-}$ mice (right) were analyzed by conventional EM. Note the ellipsoidal melanosomes (M) in RPE of *APOE*$^{+/+}$ mice and their rounder shapes in the RPE of *APOE*$^{-/-}$ mice.

(B) RPE sections from *APOE3* (left) and *APOE4* Knockin mice (right) were analyzed by conventional EM. Note the ellipsoidal melanosomes (M) in both RPE.

(C) The ratio between maximum width and length of an average of 300 melanosomes per conditions was measured using ITEM software.

(D–F) Ultrathin cryosections of RPE from *APOE3* and *APOE4* KI mice were double immunogold-labeled for PMEL luminal domain (HMB45, PAG 10) and ApoE (PAG 15). (D and E) Arrows indicate ApoE labeling in MVE and unpigmented early melanosomes (UM). (F). Arrows indicate extracellular vesicles labeled for PMEL and ApoE in the vicinity of RPE (***p < 0.01, **p < 0.02, *p < 0.05). See also Figure S4.

general loading mechanism for soluble proteins or shed luminal domains of endosomal transmembrane proteins. ApoE could also create specific regions on the membrane of ILVs and exosomes, as shown by cryo-EM that would cluster important cofactors of fibrillation. Among them, specific lipids, such as ganglioside or cholesterol, have already been reported as regulators of amyloidogenesis processes at the surface of exosomes (Yuyama et al., 2014). In view of the differential level of rescue of PMEL amyloidogenesis by *APOE3* and *APOE4* expression in vivo, the investigation of the influence of *APOE* isoforms on such processes would be of interest.

Moreover, our data suggest that the presence of ApoE in endosomes is one of the specific mechanisms that pigment cells use to avoid potential toxicity inherent to PMEL amyloidogenesis. Within MVEs, ApoE enables ILVs to nucleate newly shed PMEL prefibrillar species (Watt et al., 2011) into mature amyloid fibrils. By acting directly at the site of production of PMEL-derived amyloid peptides, ApoE would prevent the accumulation of potentially toxic PMEL-derived amyloid peptides. Interestingly, the neural crest origin of melanocytes and the analogies of trafficking and processing pathways between PMEL and APP strengthen the relevance of this process for amyloid formation in AD. In this context, however, the major expression of ApoE and Aβ by distinct cell types, astrocytes and neurons, respectively (Xu et al., 2006), prevents similar process as ApoE and Aβ would mainly encounter in the extracellular medium. It is then tempting to speculate, as observed separately for exosomes (Yuyama et al., 2014) and ApoE (Li et al., 2012), that exosomes harboring ApoE would favor endocytosis and targeting of Aβ to MVEs and provide a favorable environment for Aβ seeding and neutralization (Hu et al., 2009).

The association of ApoE with ILVs and exosomes ascertains a new pathway of secretion for ApoE that would differ from its typical release as phospholipid discs (Kockx et al., 2008). The association of ApoE with ILVs would also extend the properties of exosomes as ApoE binds specific receptors for uptake and modulates the activity of soluble ApoE receptors (Rebeck et al., 2006). This association also prompts us to reconsider the respective roles of ApoE and exosomes in several pigment cell-associated pathologies such as age-related macular degeneration (Johnson et al., 2011; Wang et al., 2009) and melanoma metastasis (Peinado et al., 2012; Pencheva et al., 2012) where ApoE may endow signaling properties to exosomes.

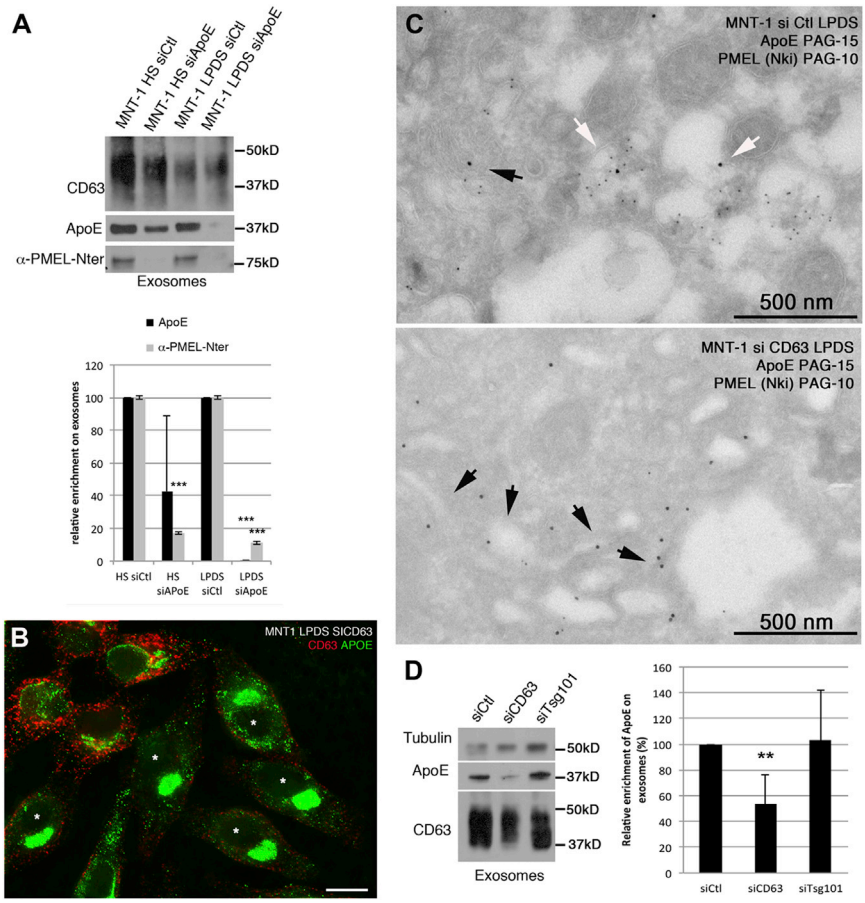

Figure 5. ApoE in CD63-Dependent Sorting of PMEL

(A) Top: exosomes from MNT-1 cells that were cultured in HS or LPDS and treated with control siRNA or ApoE siRNA were analyzed by western blot with anti-CD63, anti-ApoE, and anti PMEL luminal domain (α-PMEL-Nter antibody). Bottom: relative enrichment of ApoE and PMEL luminal domain was quantified and results are expressed as the mean ± SD of three experiments (***$p < 0.01$).

(B) MNT-1 cells in LPDS and treated with CD63 siRNA were analyzed by IFM after labeling for CD63 and ApoE. White stars indicate CD63-inactivated cells; we purposely show an experiment in which CD63 depletion was lower than normal to emphasize the differences between cells that do and do not express CD63. Scale bar, 10 μm.

(C) Ultrathin cryosections of MNT-1 cells that were cultured in LPDS and treated with control siRNA (top) or CD63 siRNA (bottom) were double immunogold labeled for PMEL luminal domain (Nki, PAG 10) and ApoE (PAG 15). White arrows indicate ApoE labeling in unpigmented melanosomes and black arrows indicate ApoE-labeling in Golgi stack.

(D) Exosomes secreted by MNT-1 cells that were cultured in LPDS and treated with control siRNA, CD63 siRNA, or tsg101 siRNA were analyzed by western blot with anti-CD63, anti-ApoE, and or anti-β-tubulin antibody as a loading control. Right: relative enrichment of ApoE was quantified and results are expressed as the mean ± SD of three experiments (**$p < 0.02$).

See also Figure S5.

EXPERIMENTAL PROCEDURES

Mice

Male *APOE*$^{-/-}$ mice (n = 3) and male C57/bl6/J (n = 3) were purchased from the Maastricht University. Mice were 12 weeks of age when sacrificed. Until sacrifice, mice were housed in cages with free access to water and regular chow diet (AB diets, Woerden). *APOE3* and *APOE4* targeted replacement mice (n = 2 each) were purchased from Taconic Europe A/S Lille Skensved. Mice were 12 weeks of age when sacrificed. Until sacrifice, mice were housed in cages with free access to water and regular chow diet (irradiated A4 from SafeDiet). Before collecting all required tissues, mice were perfused with a sterile saline solution (150 mM saline, 2.5 mM $CaCl_2$ in HEPES, pH 7.3) via the left ventricle. The eyes (enucleated and extraocular muscles were cut) were dissected and harvested in modified Karnovsky's fixative (2% paraformaldehyde/2% glutaraldehyde/0.1 m cacodylate buffer, pH 7.3/0.06% $CaCl_2$). After a few hours, eyes and skin were sectioned and fixed overnight at 4°C in modified Karnovsky's fixative. The experimental animal committee of the Maastricht University approved this animal experiment.

Cell Culture, Drug Treatment, Transfection, and siRNA Depletion

Human melanocytic MNT1 cells were maintained as previously described (van Niel et al., 2011). When indicated, fetal bovine serum was replaced by human serum and lipoprotein-depleted human serum (Millipore). Cells were treated for 24 hr with 2.5 μM GW4869 (Sigma). MNT1 cells were transfected with siRNA duplex oligonucleotides as reported previously (van Niel et al., 2011). Cells were subjected to one round of siRNA transfection and collected after 72 hr. MNT-1 cells were transfected with plasmid constructs using Lipofectamine 2000 (Invitrogen) following the manufacturer's recommendations and cells were collected and analyzed after 48 hr. For the rescue experiment, cells were subjected to two rounds of siRNA transfection against ApoE and after 72 hr cells were transfected with plasmid constructs for ApoE3 and collected after 24 hr.

Exosome Isolation

Exosomes were prepared from conditioned media incubated for 48 hr on subconfluent cells. Media were centrifuged at 2,000 × *g* for 15 min (4°C) and 4,000 × *g* (15 min, 4°C) to remove debris. Next, the supernatant was centrifuged at 10,000 × *g* for 30 min (4°C) and exosomes were collected from the supernatant by centrifugation at 100,000 × *g* for 60 min (4°C). The pellet was resuspended and washed in PBS (pH 7).

Immunoprecipitation

MNT1 cells were lysed directly in lysis buffer (20 mM Tris, 150 mM NaCl, 1% Triton X-100, 1 mM EDTA [pH 7.2]) with protease inhibitor cocktail (Roche). After 30 min at 4°C, insoluble material was removed by centrifugation at 12,000 × *g* and cell lysate was precleared for 30 min by addition of 50 μl protein G-Agarose beads (Invitrogen) and for 30 min by addition of 50 μl protein G-Agarose beads coated with irrelevant rabbit antibody (Dako). Proteins were then immunoprecipitated by adding 50 μl protein G-Agarose beads coated with antibodies in MNT-1 lysates and by adding 50 μl protein G-Agarose beads coated with specific antibody for anti-ApoE antibody in HeLa cell lysates. After 2 hr at 4°C under constant agitation, beads were washed five times in lysis buffer. The immunoprecipitates were subjected to western blot analysis as described below.

Western Blot

Triton X-100 soluble and insoluble material from MNT-1 cells was obtained as previously described (van Niel et al., 2011) and analyzed by western blot as

described in van Niel et al. (2011). Signal intensities were quantified with ImageJ software.

Electron Microscopy

Tissues from *APOE*$^{-/-}$ mice and wild-type mice and MNT-1 cells were fixed with 2.5% glutaraldehyde in 0.1 M cacodylate buffer for conventional EM analysis. Tissue and cells were processed for Epon embedding and ultrathin sections and then contrasted with uranyl acetate and lead citrate as described (Lopes et al., 2007). For ultrathin cryosectioning and immunogold labeling, samples were processed and analyzed as reported previously (van Niel et al., 2011).

Cryoelectron Microscopy

A glow-discharged lacey Formvar copper grid (Ted Pella) was loaded with 5 μl of exosome solution. Next, the solution was blotted and vitrified in liquid ethane by plunge freezing. Images were recorded under low-dose conditions with a FEI CM120 operating at 120 kV with a SSD GATAN 1 k × 1 k camera at a magnification of 35,000 resulting in 4.96 Å/pixel. The intended underfocus was set to −1.5 to −2 mm. Cryotomograms were recorded using TEMography (JEOL, USA) at 200 kV with a JEOL JEM 2200FS equipped with a Ω filter. A 10 eV energy window was used to record Z-loss filtered images. Cryotomograms were collected at 1.5° increments over 100° range at 25,000× magnification. Images were recorded at −5 to −7 μm underfocus, binning 1, corresponding to 4 Å/pixel using an Ultrascan 100 GATAN CCD camera. The total dose was set to 80 electrons/A^2. Tilt series alignment and weighted back-projection reconstruction were performed with the aid of the gold beads using *etomo* (IMOD) software. Reconstructed structures were computationally identified with the isosurface selection tool in IMOD.

Image Analysis and Quantification

Melanosome stages were defined by morphology (van Niel et al., 2011). Quantification of the length and width of melanosomes was determined using the iTEM software (Soft Imaging System [SIS]).

Antibodies list, siRNA list, exosome isolation on optiprep gradient, cell fractionation, melanin assay, genotyping, immunofluorescence microscopy, proteomic analysis, cell culture and SILAC labeling (metabolic labeling and exosome purification), in-gel digestion, liquid chromatography-tandem mass spectrometry (LC-MS/MS) analysis, and processing of MS data are described in the Supplemental Experimental Procedures.

SUPPLEMENTAL INFORMATION

Supplemental Information includes Supplemental Experimental Procedures and five figures and can be found with this article online at http://dx.doi.org/10.1016/j.celrep.2015.08.057.

AUTHOR CONTRIBUTIONS

G.v.N. conceived, designed, performed, and analyzed data from all experiments and wrote and edited the manuscript. P.B. performed and analyzed conventional electron microscopy. A.d.C. and C.F. performed cryoelectron microscopy. A.d.C. and I.H. performed cryotomography and 3D reconstruction. A.L.C. performed isolation and biochemical analysis of exosomes. R.P. performed analysis on primary melanocytes. L.S. and M.C.P. provided biopsies from mice. F.D. carried out the MS experimental work. L.D. supervised MS and proteomic data analysis. D.L. and G.R. analyzed data, wrote, and edited the manuscript. D.L. and G.R. contributed equally to this work.

ACKNOWLEDGMENTS

We are grateful to C. Delevoye (Institut Curie, UMR144) and M. Marks (Children's Hospital of Philadelphia and University of Pennsylvania) for insightful discussions and for critical reading of the manuscript, V. Fraisier and L. Sengmanivong (PICT-IBiSA Imaging Facility, Institut Curie, Paris; Nikon Imaging Center) for assistance with deconvolution microscopy, Allison de Horsey (St. George's School, Newport, RI) for critical reading and editing of the manuscript, and Gaelle Fontaine for technical assistance in genotyping. This work was supported by Institut Curie, CNRS, by the Fondation ARC pour la Recherche sur le Cancer (grant SL220100601359 to G.R.), by the Fondation pour la Recherche Médicale (to G.v.N.), by a research grant from the Amyloidosis Foundation (to G.v.N.), by the French National Research Agency through the "Investments for the Future" program (France-BioImaging, ANR-10-INSB-04), and the CelTisPhyBio Labex (ANR-10-LBX-0038) part of the IDEX PSL (ANR-10-IDEX-0001-02 PSL).

Received: November 13, 2014
Revised: July 2, 2015
Accepted: August 20, 2015
Published: September 17, 2015

REFERENCES

Brouwers, J.F., Aalberts, M., Jansen, J.W., van Niel, G., Wauben, M.H., Stout, T.A., Helms, J.B., and Stoorvogel, W. (2013). Distinct lipid compositions of two types of human prostasomes. Proteomics *13*, 1660–1666.

Conde-Vancells, J., Rodriguez-Suarez, E., Embade, N., Gil, D., Matthiesen, R., Valle, M., Elortza, F., Lu, S.C., Mato, J.M., and Falcon-Perez, J.M. (2008). Characterization and comprehensive proteome profiling of exosomes secreted by hepatocytes. J. Proteome Res. *7*, 5157–5166.

D'Andrea, M.R., Nagele, R.G., Wang, H.Y., Peterson, P.A., and Lee, D.H. (2001). Evidence that neurones accumulating amyloid can undergo lysis to form amyloid plaques in Alzheimer's disease. Histopathology *38*, 120–134.

Edgar, J.R., Eden, E.R., and Futter, C.E. (2014). Hrs- and CD63-dependent competing mechanisms make different sized endosomal intraluminal vesicles. Traffic *15*, 197–211.

Fowler, D.M., Koulov, A.V., Balch, W.E., and Kelly, J.W. (2007). Functional amyloid–from bacteria to humans. Trends Biochem. Sci. *32*, 217–224.

Haass, C., and Selkoe, D.J. (2007). Soluble protein oligomers in neurodegeneration: lessons from the Alzheimer's amyloid beta-peptide. Nat. Rev. Mol. Cell Biol. *8*, 101–112.

Harrison, R.S., Sharpe, P.C., Singh, Y., and Fairlie, D.P. (2007). Amyloid peptides and proteins in review. Rev. Physiol. Biochem. Pharmacol. *159*, 1–77.

Hellström, A.R., Watt, B., Fard, S.S., Tenza, D., Mannström, P., Narfström, K., Ekesten, B., Ito, S., Wakamatsu, K., Larsson, J., et al. (2011). Inactivation of Pmel alters melanosome shape but has only a subtle effect on visible pigmentation. PLoS Genet. *7*, e1002285.

Hoek, K.S., Schlegel, N.C., Eichhoff, O.M., Widmer, D.S., Praetorius, C., Einarsson, S.O., Valgeirsdottir, S., Bergsteinsdottir, K., Schepsky, A., Dummer, R., and Steingrimsson, E. (2008). Novel MITF targets identified using a two-step DNA microarray strategy. Pigment Cell Melanoma Res. *21*, 665–676.

Hu, X., Crick, S.L., Bu, G., Frieden, C., Pappu, R.V., and Lee, J.M. (2009). Amyloid seeds formed by cellular uptake, concentration, and aggregation of the amyloid-beta peptide. Proc. Natl. Acad. Sci. USA *106*, 20324–20329.

Ishida, B.Y., Bailey, K.R., Duncan, K.G., Chalkley, R.J., Burlingame, A.L., Kane, J.P., and Schwartz, D.M. (2004). Regulated expression of apolipoprotein E by human retinal pigment epithelial cells. J. Lipid Res. *45*, 263–271.

Ji, H., Greening, D.W., Barnes, T.W., Lim, J.W., Tauro, B.J., Rai, A., Xu, R., Adda, C., Mathivanan, S., Zhao, W., et al. (2013). Proteome profiling of exosomes derived from human primary and metastatic colorectal cancer cells reveal differential expression of key metastatic factors and signal transduction components. Proteomics *13*, 1672–1686.

Johnson, L.V., Forest, D.L., Banna, C.D., Radeke, C.M., Maloney, M.A., Hu, J., Spencer, C.N., Walker, A.M., Tsie, M.S., Bok, D., et al. (2011). Cell culture model that mimics drusen formation and triggers complement activation associated with age-related macular degeneration. Proc. Natl. Acad. Sci. USA *108*, 18277–18282.

Kanekiyo, T., Xu, H., and Bu, G. (2014). ApoE and Aβ in Alzheimer's disease: accidental encounters or partners? Neuron *81*, 740–754.

Kockx, M., Jessup, W., and Kritharides, L. (2008). Regulation of endogenous apolipoprotein E secretion by macrophages. Arterioscler. Thromb. Vasc. Biol. *28*, 1060–1067.

Krämer-Albers, E.M., Bretz, N., Tenzer, S., Winterstein, C., Möbius, W., Berger, H., Nave, K.A., Schild, H., and Trotter, J. (2007). Oligodendrocytes secrete exosomes containing major myelin and stress-protective proteins: Trophic support for axons? Proteomics Clin. Appl. *1*, 1446–1461.

Kummer, M.P., Maruyama, H., Huelsmann, C., Baches, S., Weggen, S., and Koo, E.H. (2009). Formation of Pmel17 amyloid is regulated by juxtamembrane metalloproteinase cleavage, and the resulting C-terminal fragment is a substrate for gamma-secretase. J. Biol. Chem. *284*, 2296–2306.

Li, J., Kanekiyo, T., Shinohara, M., Zhang, Y., LaDu, M.J., Xu, H., and Bu, G. (2012). Differential regulation of amyloid-β endocytic trafficking and lysosomal degradation by apolipoprotein E isoforms. J. Biol. Chem. *287*, 44593–44601.

Lopes, V.S., Wasmeier, C., Seabra, M.C., and Futter, C.E. (2007). Melanosome maturation defect in Rab38-deficient retinal pigment epithelium results in instability of immature melanosomes during transient melanogenesis. Mol. Biol. Cell *18*, 3914–3927.

Mak, A.C., Pullinger, C.R., Tang, L.F., Wong, J.S., Deo, R.C., Schwarz, J.M., Gugliucci, A., Movsesyan, I., Ishida, B.Y., Chu, C., et al. (2014). Effects of the absence of apolipoprotein e on lipoproteins, neurocognitive function, and retinal function. JAMA Neurol. *71*, 1228–1236.

Orlova, E.V., Sherman, M.B., Chiu, W., Mowri, H., Smith, L.C., and Gotto, A.M., Jr. (1999). Three-dimensional structure of low density lipoproteins by electron cryomicroscopy. Proc. Natl. Acad. Sci. USA *96*, 8420–8425.

Peinado, H., Alečković, M., Lavotshkin, S., Matei, I., Costa-Silva, B., Moreno-Bueno, G., Hergueta-Redondo, M., Williams, C., García-Santos, G., Ghajar, C., et al. (2012). Melanoma exosomes educate bone marrow progenitor cells toward a pro-metastatic phenotype through MET. Nat. Med. *18*, 883–891.

Pencheva, N., Tran, H., Buss, C., Huh, D., Drobnjak, M., Busam, K., and Tavazoie, S.F. (2012). Convergent multi-miRNA targeting of ApoE drives LRP1/LRP8-dependent melanoma metastasis and angiogenesis. Cell *151*, 1068–1082.

Raposo, G., and Marks, M.S. (2007). Melanosomes–dark organelles enlighten endosomal membrane transport. Nat. Rev. Mol. Cell Biol. *8*, 786–797.

Raposo, G., and Stoorvogel, W. (2013). Extracellular vesicles: exosomes, microvesicles, and friends. J. Cell Biol. *200*, 373–383.

Rebeck, G.W., LaDu, M.J., Estus, S., Bu, G., and Weeber, E.J. (2006). The generation and function of soluble apoE receptors in the CNS. Mol. Neurodegener. *1*, 15.

Rochin, L., Hurbain, I., Serneels, L., Fort, C., Watt, B., Leblanc, P., Marks, M.S., De Strooper, B., Raposo, G., and van Niel, G. (2013). BACE2 processes PMEL to form the melanosome amyloid matrix in pigment cells. Proc. Natl. Acad. Sci. USA *110*, 10658–10663.

Segrest, J.P., Jones, M.K., De Loof, H., Brouillette, C.G., Venkatachalapathi, Y.V., and Anantharamaiah, G.M. (1992). The amphipathic helix in the exchangeable apolipoproteins: a review of secondary structure and function. J. Lipid Res. *33*, 141–166.

Seiji, M., Fitzpatrick, T.B., Simpson, R.T., and Birbeck, M.S. (1963). Chemical composition and terminology of specialized organelles (melanosomes and melanin granules) in mammalian melanocytes. Nature *197*, 1082–1084.

Takahashi, R.H., Milner, T.A., Li, F., Nam, E.E., Edgar, M.A., Yamaguchi, H., Beal, M.F., Xu, H., Greengard, P., and Gouras, G.K. (2002). Intraneuronal Alzheimer abeta42 accumulates in multivesicular bodies and is associated with synaptic pathology. Am. J. Pathol. *161*, 1869–1879.

Thinakaran, G., and Koo, E.H. (2008). Amyloid precursor protein trafficking, processing, and function. J. Biol. Chem. *283*, 29615–29619.

Trajkovic, K., Hsu, C., Chiantia, S., Rajendran, L., Wenzel, D., Wieland, F., Schwille, P., Brügger, B., and Simons, M. (2008). Ceramide triggers budding of exosome vesicles into multivesicular endosomes. Science *319*, 1244–1247.

van Niel, G., Charrin, S., Simoes, S., Romao, M., Rochin, L., Saftig, P., Marks, M.S., Rubinstein, E., and Raposo, G. (2011). The tetraspanin CD63 regulates ESCRT-independent and -dependent endosomal sorting during melanogenesis. Dev. Cell *21*, 708–721.

Wang, A.L., Lukas, T.J., Yuan, M., Du, N., Tso, M.O., and Neufeld, A.H. (2009). Autophagy and exosomes in the aged retinal pigment epithelium: possible relevance to drusen formation and age-related macular degeneration. PLoS ONE *4*, e4160.

Watt, B., Tenza, D., Lemmon, M.A., Kerje, S., Raposo, G., Andersson, L., and Marks, M.S. (2011). Mutations in or near the transmembrane domain alter PMEL amyloid formation from functional to pathogenic. PLoS Genet. *7*, e1002286.

Watt, B., van Niel, G., Raposo, G., and Marks, M.S. (2013). PMEL: a pigment cell-specific model for functional amyloid formation. Pigment Cell Melanoma Res. *26*, 300–315.

Xu, Q., Bernardo, A., Walker, D., Kanegawa, T., Mahley, R.W., and Huang, Y. (2006). Profile and regulation of apolipoprotein E (ApoE) expression in the CNS in mice with targeting of green fluorescent protein gene to the ApoE locus. J. Neurosci. *26*, 4985–4994.

Yuyama, K., Sun, H., Sakai, S., Mitsutake, S., Okada, M., Tahara, H., Furukawa, J., Fujitani, N., Shinohara, Y., and Igarashi, Y. (2014). Decreased amyloid-β pathologies by intracerebral loading of glycosphingolipid-enriched exosomes in Alzheimer model mice. J. Biol. Chem. *289*, 24488–24498.